

## Article

# Development and Characteristic of 3D-Printable Mortar with Waste Glass Powder

Qi Deng <sup>1,†</sup>, Shuai Zou <sup>1,2,\*,†</sup>, Yonghui Xi <sup>1,\*</sup> and Amardeep Singh <sup>3</sup> 

<sup>1</sup> Department of Structural Engineering, College of Civil Engineering, Tongji University, Shanghai 200092, China

<sup>2</sup> Department of Civil and Environmental Engineering, The Hong Kong Polytechnic University, Hong Kong, China

<sup>3</sup> School of Civil Engineering & Architecture, Changzhou Institute of Technology, Changzhou 213032, China

\* Correspondence: frank-s.zou@connect.polyu.hk (S.Z.); xiyonghui@tongji.edu.cn (Y.X.)

† These authors contributed equally to this work.

**Abstract:** Three-dimensional concrete printing (3DCP) is emerging as an innovative technology and shows promise to revolutionize conventional construction modes. However, the current 3D-printed concrete (3DPC) generally requires higher cement content than conventional concrete to ensure its rheology for printing. From the perspective of cleaner production and reduce carbon emissions, this study explored the feasibility of replacing parts of cement with waste glass powder (WGP, 0%, 20%, 40%, and 60% by mass) and compared the properties of the developed 3DPC, including fluidity (flowable spread), rheology, heat of hydration, buildability, compressive strength, anisotropy, and drying shrinkage. The results showed that less than 40% WGP replacement had limited influence on the initial fluidity and static yield stress, as well as drying shrinkage, of 3DPC. Although the WGP inclusion decreased the compressive strength, it slowed down the fluidity loss and static yield stress increase, which could extend the workable time of the mixture for printing and improve buildability. The 40% WGP replacement was found increase to the buildability of the printing mixture from 150 mm to 155 mm. The printing mixture prepared with 60% WGP reduced the drying shrinkage by 50%. An exponential decay function between the fluidity and static yield stress was established so that the simple fluidity test could be used as an indicator of printability. The findings in this study provided a solution to reduce the consumption of cement in 3DPC, which could contribute to a greener production in the construction industry.



**Citation:** Deng, Q.; Zou, S.; Xi, Y.; Singh, A. Development and Characteristic of 3D-Printable Mortar with Waste Glass Powder. *Buildings* **2023**, *13*, 1476. <https://doi.org/10.3390/buildings13061476>

Academic Editor: Elena Ferretti

Received: 29 April 2023

Revised: 29 May 2023

Accepted: 4 June 2023

Published: 7 June 2023



**Copyright:** © 2023 by the authors. Licensee MDPI, Basel, Switzerland. This article is an open access article distributed under the terms and conditions of the Creative Commons Attribution (CC BY) license (<https://creativecommons.org/licenses/by/4.0/>).

**Keywords:** 3D concrete printing; waste glass powder; fresh and hardened properties; rheology; buildability; drying shrinkage

## 1. Introduction

Currently, the construction industry is one of the typical labor-intensive professions with a low automation degree and environmental pollution [1]. Under a low-carbon and sustainable development background, 3D concrete printing (3DCP) has emerged as an innovative and automatic construction method that has aroused worldwide interest in both academia and industry [2–4]. Compared with conventional construction methods, 3DCP technology is a form of additive manufacturing utilized for fabricating buildings or construction components by depositing cementitious materials layer upon layer without the use of formwork [5–7]. This concept was firstly mentioned by Pegna [8], and then developed by Khoshnevis [9] to construct large 3D structures with complex geometries through gantry robots. So far, researchers have regarded 3DCP as a cleaner production method compared with conventional construction because of its higher automation degree and reduced waste generation [10–13].

However, further examination of 3D-printable/printed mortar/concrete (3DPC) reveals it has high embodied carbon, as most of the 3DPC compositions are generally char-

acterized by a high cement content ( $830 \pm 230 \text{ kg/m}^3$ ), which is almost twice that of conventional ready-mix concrete [14,15]. Additionally, due to its high cement content and production without formwork, 3DPC has been observed to be easily cracked because of its higher drying shrinkage nature, which severely limits its practical applications [16]. In order to solve these two challenges, supplementary cementitious materials (SCMs) are therefore routinely used to partially replace cement in 3DPC mixes [17–19].

The commonly utilized SCMs, such as ground granulated blast-furnace slag (GGBS) and fly ash (FA), have attracted many researchers and already had widespread applications in the construction industry because of their positive effects on consuming waste by-products, reducing carbon dioxide emission, and improving concrete durability, etc. [20,21]. However, the supply of these conventional SCMs is becoming scarce in some regions because of changes in the industrial landscape. For example, in Hong Kong, FA supply is diminishing due to the phasing out of coal-fired power plants. Therefore, incorporating waste glass powder (WGP) as a kind of new SCM in concrete production is becoming significant and promising. As an example, the amount of glass bottles disposed of at landfills was up to 73,365 tons in Hong Kong in 2019; in other words, about 200 tons of glass bottles were dumped in landfills every day [22]. As a kind of inert material, disposal waste glass not only wastes resources but also takes up substantial landfill space. Recycling and efficiently reusing waste glass has economic and environmental values [23].

Moreover, positive effects have been found when using WGP as SCMs in concrete. Sadiqul et al. [24] partially replaced (0–25% by mass) cement with WGP for sustainable concrete practice and revealed that recycled glass mortar/concrete achieved better mechanical properties after curing for more than 90 days. The mechanism behind this was explained by the micro-size WGP's pozzolanic reaction and the formation of secondary C-S-H gels. Matos and Sousa Coutinho [25] investigated the effect of using WGP as a cement replacement (0%, 10%, and 20%) from the perspective of durability. The results indicated that the mortars containing WGP exhibited higher resistance to chloride ion penetration and remarkable resistance to sulphate attack because of the produced dense gel. The positive effect of WGP on the hardened mechanical properties and durability of mortar/concrete is also reported by other researchers (Omran and Tagnit-Hamou [26], Schwarz and Neithalath [27], Lu et al. [28], Aliabdo et al. [29], and Jiang et al. [30]).

However, using WGP as a SCM in 3D-printed concrete is a new application with associated challenges. This is because the issue in developing 3DPC lies first and foremost in its fresh properties due to the no-formwork and layer-upon-layer construction characteristics of 3DCP technology [31]. At the same time, the hardened mechanical properties of 3D-printed (3DP) products, such as compressive strength, also plays an important role in making 3DCP technology feasible in practical construction. Until now, research on incorporating WGP into 3DPC has been limited. To fill this research gap, this study explored the effect of replacing cement with different contents (0%, 20%, 40%, and 60% by mass) of WGP for 3DCP on the fluidity, setting time, rheology, and heat of hydration. The feasibility of 3D printing was evaluated by buildability with actual printing. The effect of WGP on the hardened properties including compressive strength, anisotropy, and drying shrinkage of the 3D printing mixtures was also investigated. The general relationship between fluidity and rheology of printing mixtures was revealed in this study. It is believed that our findings can provide a chance to reduce the consumption of cement in 3DCP and contribute to cleaner and greener production in the construction industry.

## 2. Materials and Methods

### 2.1. Materials and Mix Proportions

CEM I 52.5 ordinary Portland cement (OPC) utilized in this study was produced by Green Island Cement in Hong Kong. WGP was used to partially replace OPC, which was ground from waste glass cullet with a laboratory ball mill at the rotation speed of 300 r/min for 6 hours without interval in the laboratory. The waste glass cullet was sourced from waste glass bottles collected by a local glass waste recycler. Before grinding into powder,

the waste glass cullet was firstly washed, dried at 105 °C and sieved to a particle size of between 1.18 mm and 2.36 mm. The chemical compositions of CEM I 52.5 OPC and WGP were characterized by X-ray fluorescence and are listed in Table 1. The detailed particle size distributions (tested by DF-PSI Particle Size Analyzer) and morphologies are presented in Figures 1 and 2. It can be observed from Figure 2 that OPC and WGP had similar morphologies at the micrometer scale, which showed an irregular fragmented shape. Comparatively, the size of WGP was even smaller than that OPC. The mean and median particle size of WGP were shown to be 18.67  $\mu\text{m}$  and 11.15  $\mu\text{m}$ , respectively. River silica sand ranging with a particle size from 0.42 to 0.84 mm was used as aggregate for producing the printing mortar. A commercial superplasticizer and hydroxypropyl methylcellulose (HPMC) (which is a kind of viscosity modifier produced by Badische Anilin und Sodafabrik (BASF)) were used as admixtures to adjust the printability of the printing mixtures [5,32]. Since WGP also showed a hydrated cementitious property similar to cement, the dosages of admixtures were kept constant at each mix proportion so that the ratios between admixtures and binders could be kept constant. The mix proportions of the prepared printing mixtures with different contents of WGP are listed in Table 2. The mixing procedure for all of the mixtures was consistent, with 2 min dry mixing and 3 min wet mixing.

**Table 1.** Chemical compositions of OPC and WGP (mass content, %).

Material	SiO <sub>2</sub>	Al <sub>2</sub> O <sub>3</sub>	CaO	MgO	SO <sub>3</sub>	Fe <sub>2</sub> O <sub>3</sub>	K <sub>2</sub> O	Na <sub>2</sub> O	LOI
OPC	18.7	4.40	68.1	-	5.24	2.70	0.56	0.32	0.98
WGP	69.0	2.62	10.5	1.35	0.13	1.42	0.79	13.5	0.69

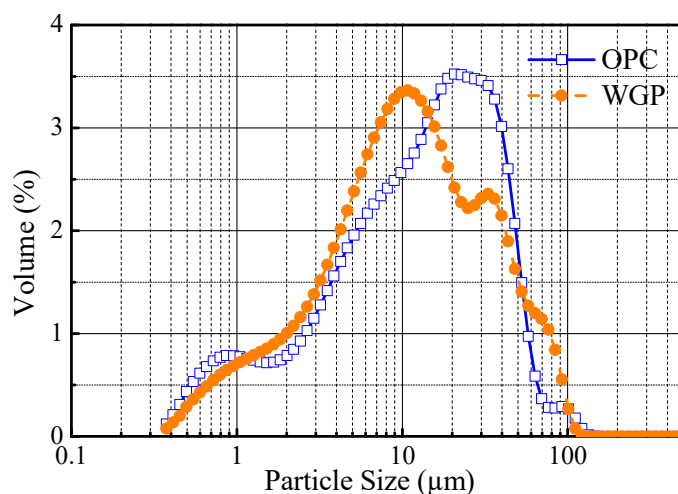


**Figure 1.** Particle size distributions of OPC and WGP.

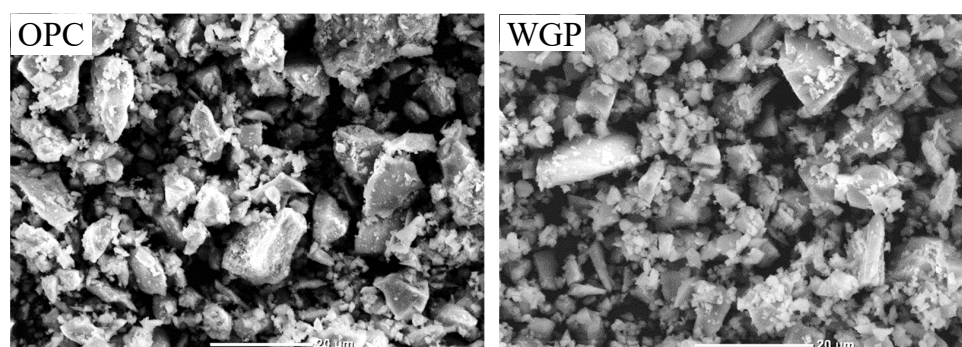


**Figure 2.** Morphologies of OPC and WGP.

**Table 2.** Mix proportions for the printing mixtures (g).

Mix	OPC	WGP	Silica Sand	Water	Superplasticizer	HPMC
M1	1000	0	1000	350	1.0	1.0
M2	800	200	1000	350	1.0	1.0
M3	600	400	1000	350	1.0	1.0
M4	400	600	1000	350	1.0	1.0

### 2.2. Three-Dimensional printer and Printing Parameters

A commercial 3D mortar printer of NELD with effective printing sizes of 600 mm × 600 mm × 600 mm in the directions of X, Y, and Z was utilized in this study. Printing was conducted by a circular nozzle with a diameter of 20 mm. Other printing parameters were set as follows: the height of each printing layer was 8 mm, the moving speed of the nozzle on the X-Y plane was 25 mm/s, and the extrusion speed of the nozzle was 4 mL/s.

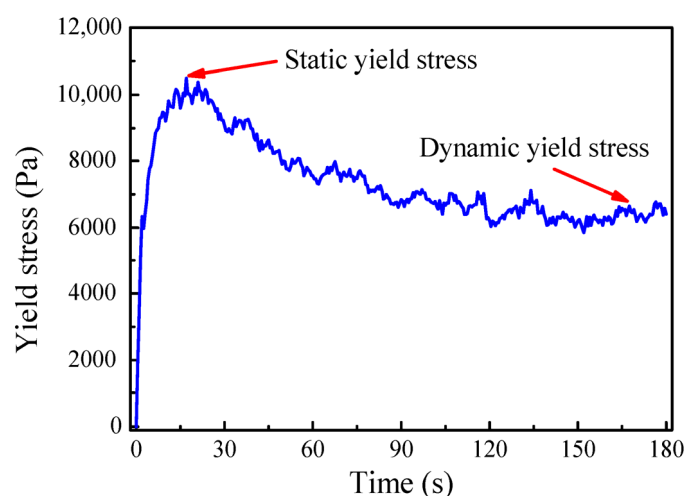
### 2.3. Experimental Methods

#### 2.3.1. Fluidity

In this study, fluidity (flowtable spread) was tested with the flow table test and recorded as the diameter (spread) of a conical sample after tumbling 25 times according to the standard (ASTM C230, 1997) [33].

#### 2.3.2. Rheological Parameters

Static yield stress, dynamic yield stress, and thixotropy were measured as rheological parameters to describe the rheological behaviors of the 3D printing mixtures. The measurements were conducted by a commercial MCR 72 rheometer of Anton Paar. Before testing, for each sample, a period of 10 s of vibration was carried out on a concrete shaking table to ensure the samples were homogeneous. After that, a 180 s constant shearing with a shearing rate of 0.2 s<sup>-1</sup> using the rheometer was performed to obtain the rheological parameters. It can be seen from a typical shear stress developing curve in Figure 3 that the peak value and equilibrium value are generally regarded as the static yield stress  $\tau_i$  and dynamic yield stress  $\tau_e$  [34]. Here, the ratio between  $\tau_i$  and  $\tau_e$  is defined as thixotropic index  $I_{thix}$ . In addition, to explore the time-dependent rheological characteristics of the 3D printing mixtures, five separate samples from the same batch were tested at 0, 30, 60, 90, and 120 min after mixing.

**Figure 3.** Typical yield stress–time curve of the 3D printing mixtures under constant shearing.

### 2.3.3. Heat of Hydration

The heat flow and cumulative heat were measured to analyze the effect of WGP contents (0%, 20%, 40%, and 60%) on the reactivity or hydration of the 3D printing mixtures. During the test, 50 g of the dry powder mixtures M1–M4 (without sand) were thoroughly mixed in an insulated container, and then, 17.5 g of water ( $w/b = 0.35$ ) were mixed with them for 1 min in the container. Subsequently, a sealed container was placed into the isothermal calorimeter (Calmetrix I-CAL HPC). The temperature of the calorimeter was kept at 20 °C and the test period was set as 72 h.

### 2.3.4. Buildability

The buildability refers to the deformation-resistance ability of the deposited 3D-printed mixtures under increasing load, which is an inherent prerequisite for the formwork-free 3DCP technology. Currently, there are still no recognized standards for the buildability of 3DPC. In this study, the buildability was tested with a commonly used method by printing the mixtures as high as possible in the form of a circle. According to previous experience [32], the buildability was assessed by the maximum printed height through printing a circular structure with a diameter of 300 mm, and each printed segment was 20 mm in width and 8 mm in height.

### 2.3.5. Compressive Strength, Anisotropy, and Drying Shrinkage

Compressive strength, anisotropy, and drying shrinkage of the 3D printing mixtures were tested to describe their hardened properties. For compressive strength and anisotropy, the specimens were prepared according to the following steps: (i) printing a rectangular slab with sizes of 300 mm, 300 mm, and 40 mm in the directions of X, Y, and Z; (ii) cutting the slab into 40 mm<sup>3</sup> cube specimens after 28 days standard curing (temperature of  $(20 \pm 2)$  °C and humidity >95%); and (iii) loading the specimens from different directions according to our previous experiments [35]. The mold-cast 40 mm<sup>3</sup> cube specimens were also measured for comparison. With the prepared specimens, the compressive strength was determined in accordance with the standard (ASTM C109, 2008) [36] and the anisotropy was assessed by the difference of the cast and printed specimens tested from different directions according to the following formula:

$$A = \frac{\sqrt{(C_X - C_C)^2 + (C_Y - C_C)^2 + (C_Z - C_C)^2}}{C_C} \quad (1)$$

in which  $A$  is the anisotropy;  $C_X$ ,  $C_Y$ , and  $C_Z$  are the compressive strength of 3D-printed specimens tested at the curing age of 28 days and loaded directions of X, Y, and Z, respectively; and  $C_C$  is the 28-day compressive strength of the cast specimen. As for the drying shrinkage, it was tested according to the standard (ASTM C157, 2017) [37] with testing specimens with the size of 285 mm × 25 mm × 25 mm and a testing period of 28 days. This was tested three times to obtain the average value of the compressive strength and drying shrinkage.

## 3. Test Results

### 3.1. Fluidity

Figure 4 shows the time-dependent properties of the 3D printing mixture with 0, 20%, 40%, and 60% of WGP. It can be observed from this figure that M1–M4 had initial fluidity values of 168 mm, 173 mm, 175 mm, and 194 mm, respectively. Fluidity of the four printing mixtures decreased with the time. The fluidity decreasing rate of WGP-incorporated printing mixtures was slower than that of pure OPC mixture. More specifically, it took 150 min for the fluidity of M2 and M3 to decrease to 140 mm, compared to 90 min for M1. The fluidity test indicated that the addition of 20% and 40% WGP had little influence on the initial fluidity, but caused a decreasing rate of fluidity with time. However, replacing cement with 60% WGP not only slowed the fluidity decreasing rate but also dramatically

increased the initial fluidity. According to previous research [38], the similar initial value and reduced decreasing rate of fluidity indicated that the 3D printing mixtures obtained a longer time span for printing. However, the largely increased initial fluidity of M4 could cause a big influence on the extrudability and buildability of the 3D printing mixtures.

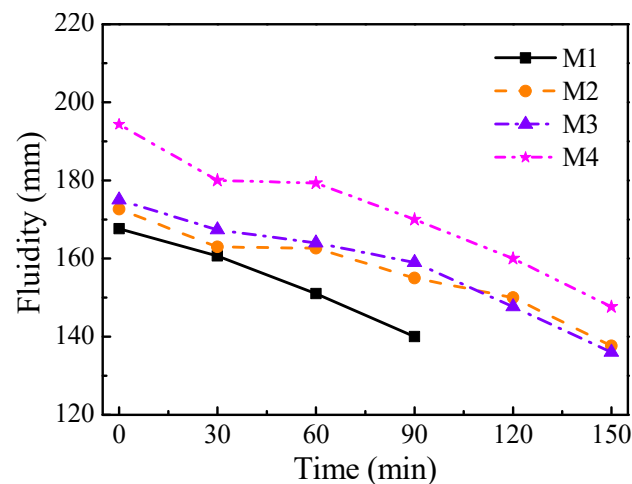


**Figure 4.** Time-dependent fluidity of 3DP mixtures with different contents of WGP.

### 3.2. Yield Stress and Thixotropy

The rheological properties, including static yield stress, dynamic yield stress, and thixotropy of the mentioned printing mixtures at different resting times (0–120 min) are presented in Figures 5 and 6 and Table 3. Figure 5 comparatively shows the yield stress–time curves of the printing mixtures M1–M4 at a resting time of 0 min to depict the effect of WGP. It can be observed that the yield stress of all of the mixtures firstly increased to different peak values and then decreased to the residual values. It should be noted that printing mixtures with 0%, 20%, and 40% WGP obtained similar peak and residual values, but significantly lower values were recorded for the 60% WGP mixtures. As reported by Zhang et al. [39], the yield stress peak was caused by the breakdown of the flocculation structure due to early-age binder hydration, and represented the static yield stress. The residual value indicated that the mixture had reached an equilibrium flow state and this value referred to the dynamic yield stress. Thus, it can be concluded that replacing cement with 40% WGP had a limited effect on the static yield stress and dynamic yield stress, while 60% WGP substitution rate decreased them greatly.

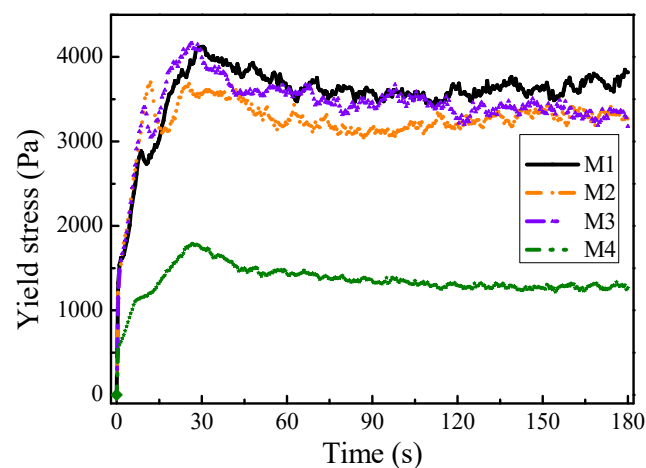


**Figure 5.** Yield stress–time curves of 3DP mixtures prepared with different WGP contents.

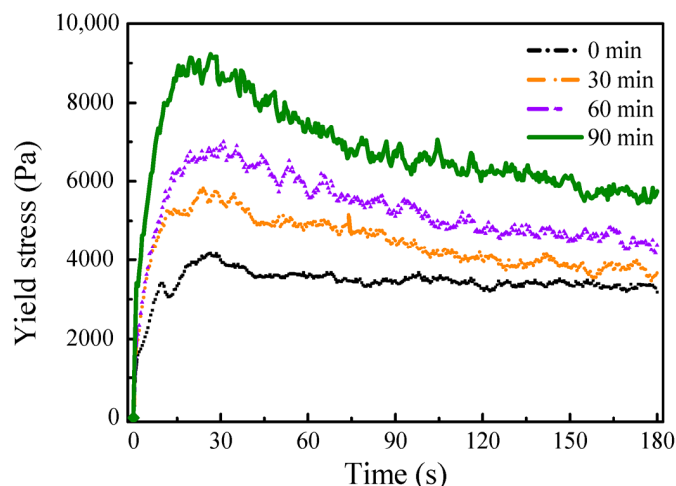


**Figure 6.** Yield stress–time curves of M3 at resting times of 0, 30, 60, and 90 min.

**Table 3.** Static and dynamic yield stress and thixotropy of mixtures.

Mix	Resting Time (min)	M1	M2	M3	M4
Static yield stress (Pa)	0	4121.4	3699.1	4147.6	1789.5
	30	7368.4	7090.2	5815.9	2847.6
	60	/	9986.5	6998.6	3250.1
	90	/	/	9164.4	4821.2
	120	/	/	/	10,162
Dynamic yield stress (Pa)	0	3589.3	3269.1	3179.1	1247.5
	30	5109.1	4714	3468.8	1398.6
	60	/	5868.2	4180	1700.1
	90	/	/	5607.4	2664.5
	120	/	/	/	6375
Thixotropy	0	1.15	1.13	1.30	1.43
	30	1.44	1.50	1.68	2.04
	60	/	1.70	1.67	1.91
	90	/	/	1.63	1.81
	120	/	/	/	1.59

Note: “/” means that the tested yield stress exceeded the equipment range.

For resting time, the static yield stress and dynamic yield stress of M3 tested at different resting times (0, 30, 60, and 90 min) are shown in Figure 6. It can be observed that the increasing trend of static yield stress with resting time was obvious, which was changed from 4147 Pa at 0 min to 9164 Pa at 90 min with an average increasing rate of 56 Pa/min. Comparatively, the corresponding increasing rate (30 Pa/min) of dynamic yield stress was much smaller. The increase of both static yield stress and dynamic yield stress could be explained by the larger hydration degree of the printing mixture. The difference in the increasing rate of static and dynamic yield stress caused the change of thixotropy of printing mixtures with time, which was shown below.

More quantitatively, the static yield stress, dynamic yield stress, and thixotropy of all the 3D printing mixtures M1~M4 tested with different resting times (0~120 min) are tabulated in Table 3. For all the specimens, their static yield stress and dynamic yield stress increased with resting time at different rates, which changed their thixotropy. Generally, the thixotropy of the printing mixtures prepared with WGP increased with time and replacing cement with WGP was found to have an enhancement effect on the thixotropy. At the resting time of 0 min, the recorded thixotropies of the printing mixtures M1 and M4 were 1.15 and 1.43, which showed an enhancement of 24.3%. This indicated that resting after mixing for a longer time and adding WGP could both help to balance the conflict between extrudability and buildability of 3D printing mixtures.

### 3.3. Heat of Hydration

Figure 7 presents the early heat evolution rate of the 3D printing mixtures prepared with different amounts of WGP. Generally, the heat evolution rate of all the mixtures increased to peak values and then decreased to low equilibrium values within one hour at which the hydration of cement enters the dormant period. As reported [40,41], this initial period referred to the dissolution period of the most reactive component such as tricalcium silicate within the cementitious binders. It can be observed from the figure that replacing cement with WGP from 0% to 60% gradually decreased the dissolution peak of the printing mixtures from 14.7 mW/g to 11.4 mW/g. This is because the addition of WGP reduced the tricalcium silicate contents in the printing mixtures [40]. Since the dissolution period was within the printability window of the printing mixtures, this can thereafter be utilized to explain the effect of WGP on workability and rheology.

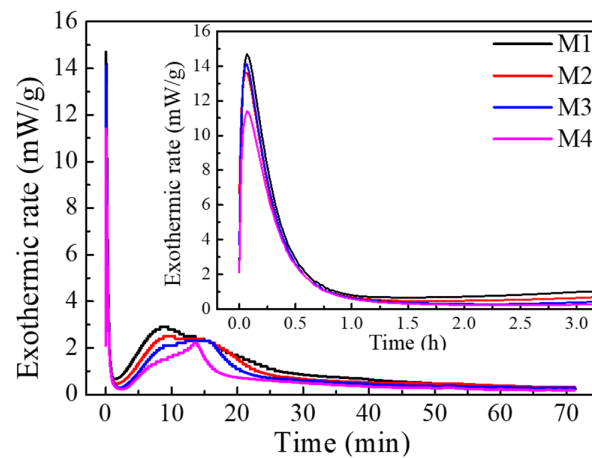


Figure 7. Heat evolution rate of M1–M4 within first 72 h.

Figure 8 shows the cumulative hydration heat of the 3D printing mixtures M1–M4 within 72 h. The cumulative hydration heat usually reflects the hydration degree of the cementitious binders [41]. It can be found from the figure that the cumulative hydration heat of printing mixtures decreased with the replacing amount of WGP and the difference increased with time, which indicated that WGP decreased the hydration of the binders of 3D printing mixtures. This result is consistent with other studies, which showed that replacing cement with waste glass powder reduced the mixed binders' hydration heat during the initial 72 h [42].

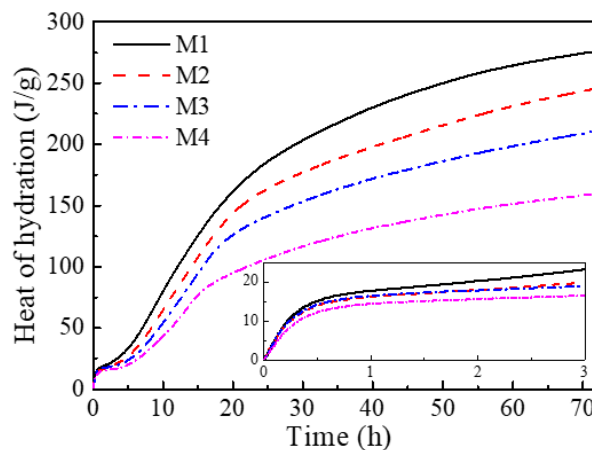
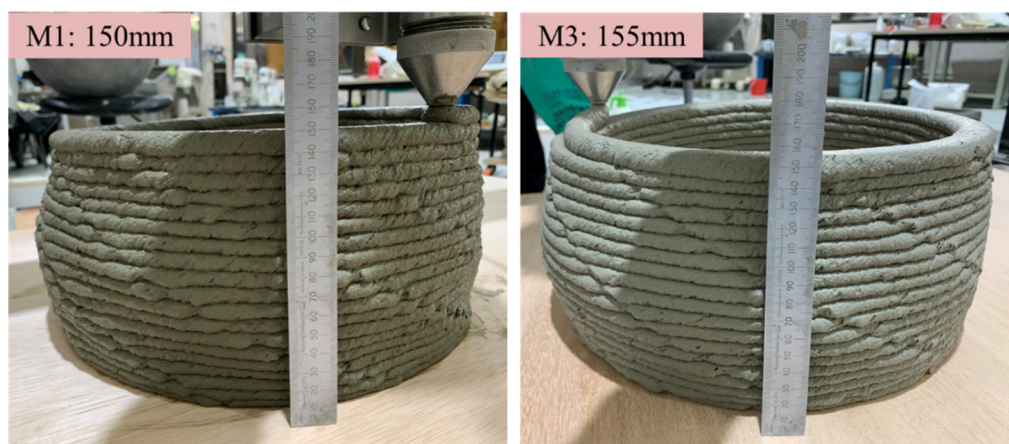


Figure 8. Cumulative hydration heat of M1–M4 within 72 h.

### 3.4. Buildability

It should be pointed out that only M1 and M3 were tested for buildability. Comparatively, M2 with 20% WGP had limited influence on the fluidity and rheology of printing mixtures; at the same time, M4 with 60% WGP significantly changed the initial fluidity and static yield stress of the printing mixture, which was predicted to have a big negative influence on the buildability of the printing mixtures. The buildability testing results are shown in Figure 9 and it can be seen that the maximum printing heights of M1 and M3 were 150 mm and 155 mm, respectively. This indicated that replacing cement with 40% WGP could improve the buildability and proved that WGP showed a positive effect on 3D concrete printing from the perspective of printability. This result was also consistent with the testing result of static yield stress (which is regarded as the indicator of buildability), which increased from 4121.4 Pa to 4147.6 Pa after replacing cement with 40% WGP.



**Figure 9.** Maximum printing height of 3D printing mixtures M1 and M3.

### 3.5. Compressive Strength

The compressive strength at curing times of 1, 7, and 28 days of the 3DP specimens with 0%, 20%, 40%, and 60% WGP were presented in Figure 10. It can be observed that WGP had negative effects on the compressive strength development of the 3DP specimens. By replacing 60% of cement with WGP, the compressive strength of 3DP specimens M1–M4 decreased from 24.8 MPa to 6.8 MPa at 1 day, from 42.9 MPa to 18.6 MPa at 7 days, and from 48.6 MPa to 25.3 MPa at 28 days. This indicated that the addition of WGP decreased the strength development and the final compressive strength within 28 days of curing. The decrease in the compressive strength is attributed to the decreased cement content and explained by the inferior hydration behavior of water glass powder than cement, which can be proved by the cumulative heat release of the 3D printing mixtures incorporated with WGP. This is because the WGP of this study (same source, grain size, and preparing steps used by the authors' research group previously) attained moderate reactivity [43]. However, it should be noted that studies have indicated that replacing cement with suitable content of WGP could improve compressive strength, especially under the development of ultra-high-performance concrete with seawater [44,45]. These phenomena were explained by the low water/binder, long-term curing condition, and the marine metal ions, which showed that WGP could serve as a filler and act as a pozzolanic material to improve the compressive strength. However, in this study, under the 0.35 water/binder ratio and 28 days standard curing, the negative effect of WGP on compressive strength was observed.

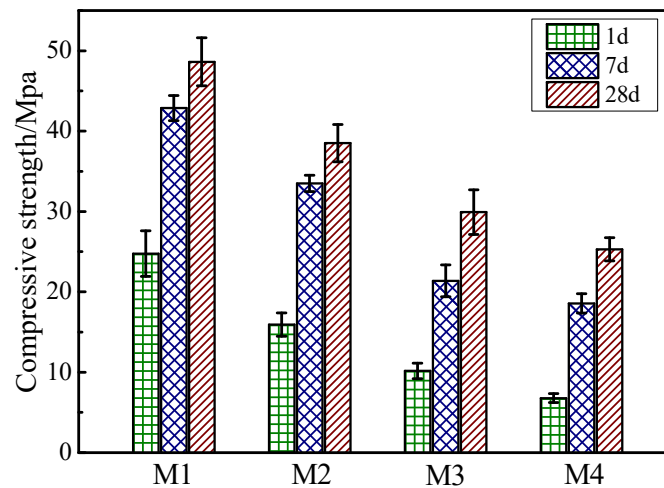


**Figure 10.** Compressive strength of 3DP specimens with 0~60% WGP at curing times of 1, 7, and 28 days.

### 3.6. Anisotropy

Anisotropy is a special property of 3D-printed products, which is caused by its layer-upon-layer printing feature. In this study, the compressive strength of the printed samples (28 days) loaded in different directions with 0% and 40% WGP are presented in Figure 11. It can be found that the compressive strength of 3D-printed mortar with/without WGP had obvious anisotropy. The highest compressive strengths were generally in the Y direction in this study, which was even higher than the value of the mold-cast sample. The lowest compressive strengths appeared to be at the loading direction of Z. Taking M1 as an example, the highest and lowest compressive strengths were 55.9 MPa in the Y direction and 37.0 MPa in the Z direction. According to the anisotropy index calculation method shown in Formula (1), the anisotropy index of the printing mixtures with 0% and 40% WGP were 0.31 and 0.36, respectively, which indicated that WGP slightly increased the anisotropy on the compressive strength of the 3D printing mixtures.

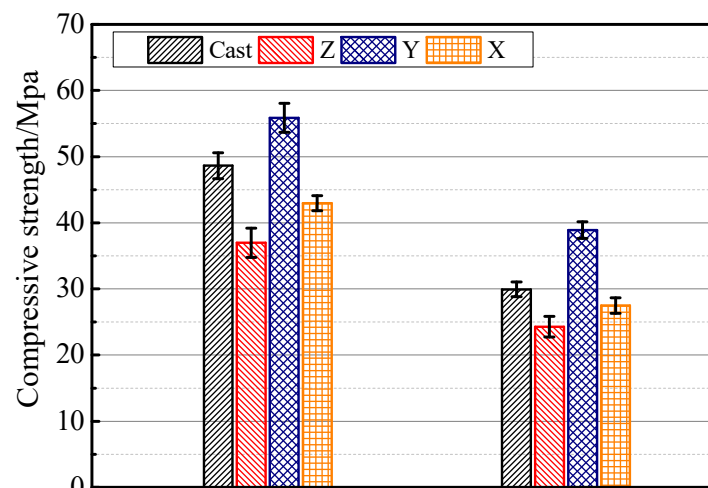


**Figure 11.** Compressive strength of M1 and M3 specimens with different loading directions [35].

### 3.7. Drying Shrinkage

The drying shrinkage testing results of the 3D-printed mixtures with various dosages of WGP are shown in Figure 12. It can be observed from this figure that the drying shrinkage of the printing mixtures with different contents of WGP all sharply increased during the first seven days and then tended to moderate. Comparatively, the 28-day drying shrinkages of printing mixtures M1~M4 were 1198  $\mu\epsilon$ , 1102  $\mu\epsilon$ , 1008  $\mu\epsilon$ , and 680  $\mu\epsilon$ ,

respectively, which indicated that replacing cement with WGP could reduce the drying shrinkage of the printing mixtures and that a 43.2% reduction was achieved by 60% WGP replacement. Generally, the glass showed alkali–silica reaction (ASR) when utilized in mortar/concrete and this ASR expansion effect would partially offset the drying shrinkage of mortar/concrete [46,47]. The particle size range in which glass began to reduce ASR was ambiguous because different studies provided different ranges; however, a general average particle size in which reduction in ASR can begin to be seen is below 1 mm [48]. In this study, since the size of the most parts of WGP was under 75  $\mu\text{m}$ , we could therefore ignore the offset effect of ASR on the drying shrinkage. Thus, in this study, the benefit of WGP on the drying shrinkage reduction can be attributed to the promoting effect of WGP on the pore structure of mortar/concrete because of its filling effect and pozzolanic reaction. Similar positive effects of WGP on the drying shrinkage reduction of mortar/concrete were also found by other researchers [49,50].

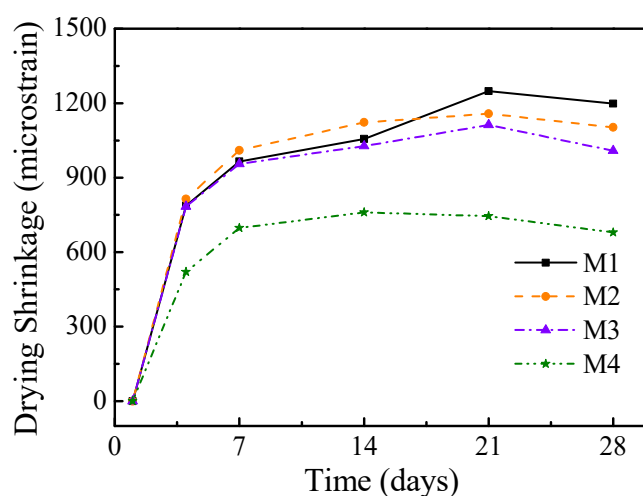


Figure 12. Drying shrinkage behavior of 3DP mixtures with different contents of WGP.

#### 4. Relationship between Fluidity and Rheology

Fresh property is comparatively more important for 3DP concrete than conventional concrete because it affects printability. Fluidity and rheology are often studied together as important parts of the 3DCP-related studies to evaluate printability. Comparatively, fluidity is easier to test and also shows operational sensitivity. In contrast, the rheology test is more accurate and scientific for assessing the fresh properties of 3DCP; however, it requires special experimental instrumentation and is difficult to utilize on-site. Since both fluidity and rheology have a strong relationship with printability, it is believed that there is a certain relationship between fluidity and rheology.

Figure 13 shows the relationship and fitting curve between the fluidity and static yield stress of mixtures M1–M4. The fluidity was negatively correlated with the static yield stress. Meanwhile, the amount of WGP was found to have a slight impact on this relationship. Taking the fluidity at around 160 mm and 168 mm as examples, it can be observed that the static yield stress increased with the WGP content when the mixtures had similar fluidity. Additionally, taking the static yield stress of 4000 Pa as an example, it can be observed that the higher the WGP content, the higher the fluidity of the printing mixtures. These results are consistent with the buildability testing result, which showed that M3 prepared with 40% WGP had a better printability than M1 without WGP. The mechanism behind it was probably because of the increased static yield stress at a similar fluidity.

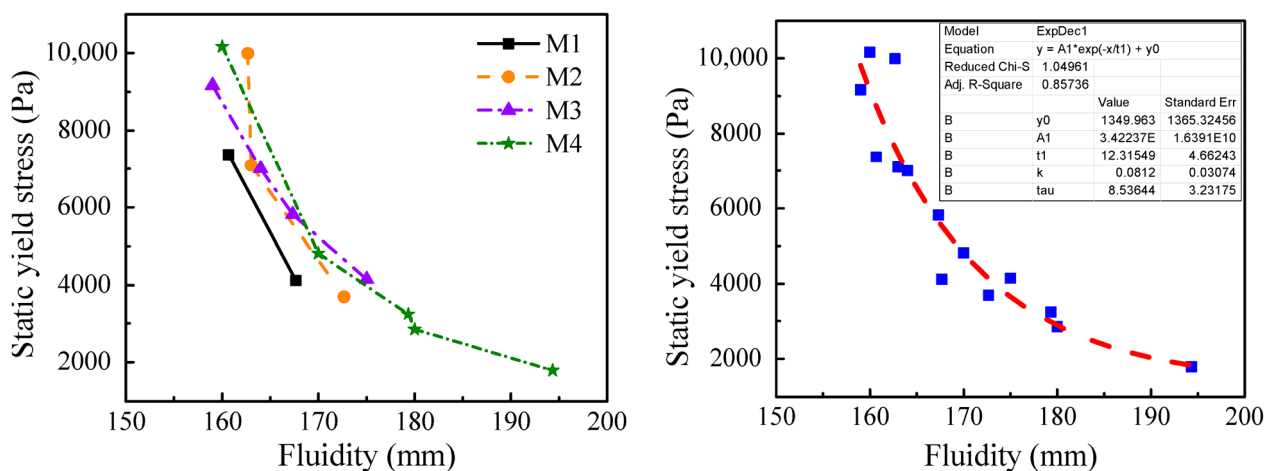


Figure 13. Relationship between fluidity and static yield stress of mixtures M1–M4.

Furthermore, when all of the points of M1~M4 were fitted to explore the quantitative relationship between fluidity and the static yield stress. An exponential decay relationship can be found. When the fluidity was in the range from 155 mm to 195 mm and the static yield stress was in the range from 1000 Pa to 10,000 Pa, the relationship between the static yield stress ( $Y_{sys}$ ) and fluidity ( $X_f$ ) could be described by the following relationship:

$$Y_{sys} = 3.4 * \exp(-X_f/12.3) + 1350 \tag{2}$$

### 5. Discussion

#### 5.1. Fresh Properties

According to the above results, it was found that the incorporation of WGP had an influence on the fresh properties of the 3D printing mixtures. Generally, WGP not only improved its initial fluidity value but also reduced its decreasing rate with time. As for the rheology, the effect of WGP was similar to that of fluidity. Specifically, replacing cement with less than 40% WGP had a limited effect on the static yield stress and dynamic yield stress, while the 60% WGP substitution rate decreased them significantly. As previously reported [51], the fluidity and rheology are mainly influenced by the flocculation structure formed by the binder dissolution and hydration when the parameters of aggregate and water are constant. Thus, the effect can be explained from the point of view of heat of hydration testing results.

It was found that WGP decreased both the initial exothermic peak intensity and cumulative heat release of the 3D printing mixtures within the first three hours, which indicated that WGP-incorporated mixtures had a weaker early hydration dissolution and activity, and it therefore explained the increase of fluidity, slowing down of the fluidity decreasing rate, and decrease of the static yield stress. However, it should be noted that when the cement replacing rate was less than or equal to 40%, the differences between the exothermic heat peak of the three mixtures were slight. This indicated that the amount of binder dissolution and the dense degree of the formed flocculation structure were similar in these three printing mixtures, which thereafter explained that the initial fluidity and static yield stress of the mixtures prepared with 20% and 40% WGP were similar to the cement mixture reference. However, when the cement replacing rate reached 60%, the exothermic peak showed a significant decrease, indicating that there was a decrease in the amount of binder dissolution and dense degree of the flocculation structure, which therefore caused the high increase in the initial fluidity and decrease of the initial static yield stress.

Except for the flocculation structure formed by the binder dissolution and hydration, the fluidity and rheology were also influenced by the colloidal interaction between particles, which was highly dependent on the volume fraction, bulk density, and particle size of the binder particles [52]. As described in Figure 1, the particle size of WGP was smaller than

cement, indicating its larger surface area, which could help increase the colloidal interaction between particles and thereafter decrease the fluidity and improve the static yield stress [53]. This also helped to explain that there was not much difference in the fluidity and static yield stress when the WGP substituting ratio was no more than 40% due to the offset effect of the decreased chemical flocculation and increased physical colloidal interaction. However, the physical colloidal interaction was much weaker than the chemical flocculation structure; thus, it could not change the influence caused by reduced flocculation structure formation when the WGP replacing rate was 60%.

### 5.2. Buildability and Hardened Properties

In terms of buildability, the similar initial static yield stress implied that replacing 40% cement with WGP had limited influence on the buildability, which was confirmed by the buildability test of the printing mixtures M1 and M3. Meanwhile, the slowing down of fluidity decreasing rate implied that adding 40% WGP could extend the workable printing time of the mixtures. Thus, from the perspective of fresh properties and buildability, replacing cement with WGP is beneficial for 3D printing when the substituting rate is no more than 40%. However, as for the hardened properties, this study found that WGP had a large negative effect on the compressive strength development. At curing ages of 1, 7, and 28 days, there was a respective 58.9%, 50.1%, and 38.5% decrease of compressive strength with a 40% replacement of cement. The decrease in the compressive strength could be explained by the decreased cumulative heat release of the 3D printing mixtures incorporated with WGP. A positive effect on drying shrinkage of replacing cement with WGP only appeared at 60% replacement rate. Thus, other methods should be explored to make up the loss of mechanical properties and help control of drying shrinkage of the printing mixtures when incorporating WGP into 3DCP.

### 5.3. Relationship between Fluidity and Static Yield Stress

In the case of the investigation of the relationship between fluidity and static yield stress, an exponential decay function was provided in this study. Generally, the fluidity tested by the flow table is operation-sensitive and therefore lacks accuracy, but it is easy to operate and suitable for testing and judging the state of concrete on site. On the contrary, although rheology is more accurate and scientific, it is hard to operate on site. It has been reported that rheology plays an important role in deciding the printability of 3DPC and some studies have tried to explore and build a relationship between rheology and printability. For example, Roussel [51] discussed the rheological requirements needed to control the final geometrical dimensions of one layer and of the entire object, including buckling stability and surface cracking. The research of Kruger et al. [54] presented an analytical model based on the novel rheological characteristics of materials as a method for quantifying the buildability performance of a 3D-printable concrete/mortar. In this study, the easily tested fluidity parameter could provide information on the rheology and printability, and help to set up reasonable printing parameters such as the thickness of the single printed layer, the maximum total printing height, the moving speed of printing head, and the minimum printing time of per layer, which could provide a guideline for practical printing.

## 6. Conclusions

In the study, WGP was used as a replacement of cement to produce greener 3DPC. Properties of the 3DPC with different WGP contents (0%, 20%, 40%, and 60% by mass) were comparatively explored, including fluidity, static yield stress, dynamic yield stress, thixotropy, heat of hydration, buildability, compressive strength, anisotropy, and drying shrinkage. The relationship between fluidity and rheology of the printing mixtures was revealed. According to the experimental results and discussions, the following conclusions can be drawn:

- (1) Less than 40% replacement of cement by WGP had a limited influence on the initial fluidity, initial static yield stress, buildability, and drying shrinkage of the 3D printing mixture. Although it decreased the compressive strength, it slowed down the fluidity decrease and static yield stress increase, which could extend the open printing time of the mixture and was therefore regarded to be beneficial from the perspective of printing.
- (2) The printing mixture prepared with 60% WGP reduced the drying shrinkage by 50%. However, it significantly decreased the initial fluidity, initial static yield stress, buildability, and compressive strength of the printing mixture.
- (3) An exponential decay function between fluidity and static yield stress was provided. Based on this, the simple fluidity test could provide information on the printability of printing mixtures and help to set up reasonable printing parameters to guide practical printing.

**Author Contributions:** Q.D.: Methodology, Investigation, Writing—Reviewing and Editing. S.Z.: Methodology, Data curation, Investigation, Writing—Original draft. Y.X.: Methodology, Writing—Reviewing and Editing, Supervision. A.S.: Writing—Reviewing and Editing and Methodology. All authors have read and agreed to the published version of the manuscript.

**Funding:** This research received no external funding.

**Data Availability Statement:** Data available on request due to restrictions eg privacy or ethical.

**Acknowledgments:** The support from National Key R&D Program of China (2022YFE0198300) and Shanghai Science and Technology Commission Innovation Action Plan (22dz1207300) is highly acknowledged.

**Conflicts of Interest:** The authors declare no conflict of interest.

## References

1. Yuan, H.; Shen, L. Trend of the research on construction and demolition waste management. *Waste Manag.* **2011**, *31*, 670–679. [[CrossRef](#)] [[PubMed](#)]
2. Xiao, J.; Ji, G.; Zhang, Y.; Ma, G.; Mechtcherine, V.; Pan, J.; Wang, L.; Ding, T.; Duan, Z.; Du, S. Large-scale 3D printing concrete technology: Current status and future opportunities. *Cem. Concr. Compos.* **2021**, *122*, 104115. [[CrossRef](#)]
3. Buswell, R.A.; Leal de Silva, W.R.; Jones, S.Z.; Dirrenberger, J. 3D printing using concrete extrusion: A roadmap for research. *Cem. Concr. Res.* **2018**, *112*, 37–49. [[CrossRef](#)]
4. Panda, B.; Tan, M.J. Experimental study on mix proportion and fresh properties of fly ash based geopolymer for 3D concrete printing. *Ceram. Int.* **2018**, *44*, 10258–10265. [[CrossRef](#)]
5. Xiao, J.; Zou, S.; Yu, Y.; Wang, Y.; Ding, T.; Zhu, Y.; Yu, J.; Li, S.; Duan, Z.; Wu, Y.; et al. 3D recycled mortar printing: System development, process design, material properties and on-site printing. *J. Build. Eng.* **2020**, *32*, 101779. [[CrossRef](#)]
6. Mohan, M.K.; Rahul, A.V.; De Schutter, G.; Van Tittelboom, K. Extrusion-based concrete 3D printing from a material perspective: A state-of-the-art review. *Cem. Concr. Compos.* **2021**, *115*, 103855. [[CrossRef](#)]
7. Heidarneshad, F.; Zhang, Q. Shotcrete based 3D concrete printing: State of art, challenges, and opportunities. *Constr. Build. Mater.* **2022**, *323*, 126545. [[CrossRef](#)]
8. Pegna, J. Exploratory investigation of solid freeform construction. *Autom. Constr.* **1997**, *5*, 427–437. [[CrossRef](#)]
9. Khoshnevis, B. Automated construction by contour crafting—Related robotics and information technologies. *Autom. Constr.* **2004**, *13*, 5–19. [[CrossRef](#)]
10. Weng, Y.; Li, M.; Ruan, S.; Wong, T.N.; Tan, M.J.; Ow Yeong, K.L.; Qian, S. Comparative economic, environmental and productivity assessment of a concrete bathroom unit fabricated through 3D printing and a precast approach. *J. Clean. Prod.* **2020**, *261*, 121245. [[CrossRef](#)]
11. Han, Y.; Yang, Z.; Ding, T.; Xiao, J. Environmental and economic assessment on 3D printed buildings with recycled concrete. *J. Clean. Prod.* **2021**, *278*, 123884. [[CrossRef](#)]
12. De Schutter, G.; Lesage, K.; Mechtcherine, V.; Nerella, V.N.; Habert, G.; Agusti-Juan, I. Vision of 3D printing with concrete—Technical, economic and environmental potentials. *Cem. Concr. Res.* **2018**, *112*, 25–36. [[CrossRef](#)]
13. Nerella, V.N.; Krause, M.; Mechtcherine, V. Direct printing test for buildability of 3D-printable concrete considering economic viability. *Autom. Constr.* **2020**, *109*, 102986. [[CrossRef](#)]
14. Wang, L.; Ma, H.; Li, Z.; Ma, G.; Guan, J. Cementitious composites blending with high belite sulfoaluminate and medium-heat Portland cements for largescale 3D printing. *Addit. Manuf.* **2021**, *46*, 102189. [[CrossRef](#)]
15. Zhang, C.; Nerella, V.N.; Krishna, A.; Wang, S.; Zhang, Y.; Mechtcherine, V.; Banthia, N. Mix design concepts for 3D printable concrete: A review. *Cem. Concr. Compos.* **2021**, *122*, 104155. [[CrossRef](#)]

16. Zhang, H.; Xiao, J. Plastic shrinkage and cracking of 3D printed mortar with recycled sand. *Constr. Build. Mater.* **2021**, *302*, 124405. [[CrossRef](#)]
17. Liu, S.; Lu, B.; Li, H.; Pan, Z.; Jiang, J.; Qian, S. A comparative study on environmental performance of 3D printing and conventional casting of concrete products with industrial wastes. *Chemosphere* **2022**, *298*, 134310. [[CrossRef](#)]
18. Bhattacharjee, S.; Basavaraj, A.S.; Rahul, A.V.; Santhanam, M.; Gettu, R.; Panda, B.; Schlangen, E.; Chen, Y.; Copuroglu, O.; Ma, G.; et al. Sustainable materials for 3D concrete printing. *Cem. Concr. Compos.* **2021**, *122*, 104156. [[CrossRef](#)]
19. Dey, D.; Srinivas, D.; Panda, B.; Suraneni, P.; Sitharam, T.G. Use of industrial waste materials for 3D printing of sustainable concrete: A review. *J. Clean. Prod.* **2022**, *340*, 130749. [[CrossRef](#)]
20. Juenger, M.C.G.; Siddique, R. Recent advances in understanding the role of supplementary cementitious materials in concrete. *Cem. Concr. Res.* **2015**, *78*, 71–80. [[CrossRef](#)]
21. Skibsted, J.; Snellings, R. Reactivity of supplementary cementitious materials (SCMs) in cement blends. *Cem. Concr. Res.* **2019**, *124*, 105799. [[CrossRef](#)]
22. Lu, J.-X.; Shen, P.; Zheng, H.; Zhan, B.; Ali, H.A.; He, P.; Poon, C.S. Synergetic recycling of waste glass and recycled aggregates in cement mortars: Physical, durability and microstructure performance. *Cem. Concr. Compos.* **2020**, *113*, 103632. [[CrossRef](#)]
23. Dong, W.; Li, W.; Tao, Z. A comprehensive review on performance of cementitious and geopolymeric concretes with recycled waste glass as powder, sand or cullet. *Resour. Conserv. Recycl.* **2021**, *172*, 105664. [[CrossRef](#)]
24. Islam, G.M.S.; Rahman, M.H.; Kazi, N. Waste glass powder as partial replacement of cement for sustainable concrete practice. *Int. J. Sustain. Built Environ.* **2017**, *6*, 37–44. [[CrossRef](#)]
25. Matos, A.M.; Sousa-Coutinho, J. Durability of mortar using waste glass powder as cement replacement. *Constr. Build. Mater.* **2012**, *36*, 205–215. [[CrossRef](#)]
26. Omran, A.; Tagnit-Hamou, A. Performance of glass-powder concrete in field applications. *Constr. Build. Mater.* **2016**, *109*, 84–95. [[CrossRef](#)]
27. Schwarz, N.; Neithalath, N. Influence of a fine glass powder on cement hydration: Comparison to fly ash and modeling the degree of hydration. *Cem. Concr. Res.* **2008**, *38*, 429–436. [[CrossRef](#)]
28. Lu, J.-X.; Zhou, Y.; He, P.; Wang, S.; Shen, P.; Poon, C.S. Sustainable reuse of waste glass and incinerated sewage sludge ash in insulating building products: Functional and durability assessment. *J. Clean. Prod.* **2019**, *236*, 117635. [[CrossRef](#)]
29. Aliabdo, A.A.; Abd Elmoaty, A.E.M.; Aboshama, A.Y. Utilization of waste glass powder in the production of cement and concrete. *Constr. Build. Mater.* **2016**, *124*, 866–877. [[CrossRef](#)]
30. Jiang, X.; Xiao, R.; Bai, Y.; Huang, B.; Ma, Y. Influence of waste glass powder as a supplementary cementitious material (SCM) on physical and mechanical properties of cement paste under high temperatures. *J. Clean. Prod.* **2022**, *340*, 130778. [[CrossRef](#)]
31. Rollakanti, C.R.; Prasad, C.V.S.R. Applications, performance, challenges and current progress of 3D concrete printing technologies as the future of sustainable construction—A state of the art review. *Mater. Today Proc.* **2022**, *65*, 995–1000. [[CrossRef](#)]
32. Zou, S.; Xiao, J.; Duan, Z.; Ding, T.; Hou, S. On rheology of mortar with recycled fine aggregate for 3D printing. *Constr. Build. Mater.* **2021**, *311*, 125312. [[CrossRef](#)]
33. ASTM C230/C230M-14; Standard Specification for Flow Table for Use in Tests of Hydraulic Cement. ASTM International: West Conshohocken, PA, USA, 2014.
34. Qian, Y.; Kawashima, S. Distinguishing dynamic and static yield stress of fresh cement mortars through thixotropy. *Cem. Concr. Compos.* **2018**, *86*, 288–296. [[CrossRef](#)]
35. Ding, T.; Xiao, J.; Zou, S.; Wang, Y. Hardened properties of layered 3D printed concrete with recycled sand. *Cem. Concr. Compos.* **2020**, *113*, 103724. [[CrossRef](#)]
36. ASTM C109/C109M; Standard Test Method for Comprehensive Strength of Hydraulic Cement Mortars. ASTM International: West Conshohocken, PA, USA, 2013.
37. ASTM C157/C157M-08; Standard Test Method for Length Change of Hardened Hydraulic-Cement Mortar and Concrete. ASTM International: West Conshohocken, PA, USA, 2014.
38. Zou, S.; Xiao, J.; Ding, T.; Duan, Z.; Zhang, Q. Printability and advantages of 3D printing mortar with 100% recycled sand. *Constr. Build. Mater.* **2021**, *273*, 121699. [[CrossRef](#)]
39. Zhang, C.; Deng, Z.; Chen, C.; Zhang, Y.; Mechtcherine, V.; Sun, Z. Predicting the static yield stress of 3D printable concrete based on flowability of paste and thickness of excess paste layer. *Cem. Concr. Compos.* **2022**, *129*, 104494. [[CrossRef](#)]
40. Zheng, D.; Wang, D.; Cui, H.; Chen, X. Hydration characteristics of cement with high volume circulating fluidized bed fly ash. *Constr. Build. Mater.* **2023**, *380*, 131310. [[CrossRef](#)]
41. Xu, Z.; Gao, J.; Zhao, Y.; Li, S.; Guo, Z.; Luo, X.; Chen, G. Promoting utilization rate of ground granulated blast furnace slag (GGBS): Incorporation of nanosilica to improve the properties of blended cement containing high volume GGBS. *J. Clean. Prod.* **2022**, *332*, 130096. [[CrossRef](#)]
42. Liu, G.; Florea, M.V.A.; Brouwers, H.J.H. The hydration and microstructure characteristics of cement pastes with high volume organic-contaminated waste glass powder. *Constr. Build. Mater.* **2018**, *187*, 1177–1189. [[CrossRef](#)]
43. Lu, J.-X.; Shen, P.; Zheng, H.; Ali, H.A.; Poon, C.S. Development and characteristics of ultra high-performance lightweight cementitious composites (UHP-LCCs). *Cem. Concr. Res.* **2021**, *145*, 106462. [[CrossRef](#)]
44. Salahaddin, S.D.; Haido, J.H.; Wardeh, G. The behavior of UHPC containing recycled glass waste in place of cementitious materials: A comprehensive review. *Case Stud. Constr. Mater.* **2022**, *17*, e01494. [[CrossRef](#)]

45. He, Z.-H.; Han, X.-D.; Zhang, M.-Y.; Yuan, Q.; Shi, J.-Y.; Zhan, P.-M. A novel development of green UHPC containing waste concrete powder derived from construction and demolition waste. *Powder Technol.* **2022**, *398*, 117075. [[CrossRef](#)]
46. Liu, Z.; Shi, C.; Shi, Q.; Tan, X.; Meng, W. Recycling waste glass aggregate in concrete: Mitigation of alkali-silica reaction (ASR) by carbonation curing. *J. Clean. Prod.* **2022**, *370*, 133545. [[CrossRef](#)]
47. He, P.; Zhang, B.; Lu, J.-X.; Poon, C.S. Reaction mechanisms of alkali-activated glass powder-ggbs-CAC composites. *Cem. Concr. Compos.* **2021**, *122*, 104143. [[CrossRef](#)]
48. Bueno, E.T.; Paris, J.M.; Clavier, K.A.; Spreadbury, C.; Ferraro, C.C.; Townsend, T.G. A review of ground waste glass as a supplementary cementitious material: A focus on alkali-silica reaction. *J. Clean. Prod.* **2020**, *257*, 120180. [[CrossRef](#)]
49. Abellan-Garcia, J.; Iqbal Khan, M.; Abbas, Y.M.; Martínez-Lirón, V.; Carvajal-Muñoz, J.S. The drying shrinkage response of recycled-waste-glass-powder-and calcium-carbonate-based ultrahigh-performance concrete. *Constr. Build. Mater.* **2023**, *379*, 131163. [[CrossRef](#)]
50. Chen, X.; Chen, H.; Tan, W. Effect of glass powder on the mechanical and drying shrinkage of glass-fiber-reinforced cementitious composites. *Case Stud. Constr. Mater.* **2022**, *17*, e01587. [[CrossRef](#)]
51. Roussel, N. Rheological requirements for printable concretes. *Cem. Concr. Res.* **2018**, *112*, 76–85. [[CrossRef](#)]
52. Ma, S.; Qian, Y.; Kawashima, S. Experimental and modeling study on the non-linear structural build-up of fresh cement pastes incorporating viscosity modifying admixtures. *Cem. Concr. Res.* **2018**, *108*, 1–9. [[CrossRef](#)]
53. Long, W.-J.; Tao, J.-L.; Lin, C.; Gu, Y.-c.; Mei, L.; Duan, H.-B.; Xing, F. Rheology and buildability of sustainable cement-based composites containing micro-crystalline cellulose for 3D-printing. *J. Clean. Prod.* **2019**, *239*, 118054. [[CrossRef](#)]
54. Kruger, J.; Zeranka, S.; van Zijl, G. 3D concrete printing: A lower bound analytical model for buildability performance quantification. *Autom. Constr.* **2019**, *106*, 102904. [[CrossRef](#)]

**Disclaimer/Publisher's Note:** The statements, opinions and data contained in all publications are solely those of the individual author(s) and contributor(s) and not of MDPI and/or the editor(s). MDPI and/or the editor(s) disclaim responsibility for any injury to people or property resulting from any ideas, methods, instructions or products referred to in the content.